Biochemistry

Article

Cite This: Biochemistry XXXX, XXX, XXX-XXX

pubs.acs.org/biochemistry

# A Kinetic Model of Nonenzymatic RNA Polymerization by Cytidine-5′-phosphoro-2-aminoimidazolide

Travis Walton and Jack W. Szostak*

Howard Hughes Medical Institute, Department of Molecular Biology, and Center for Computational and Integrative Biology, Massachusetts General Hospital, Boston, Massachusetts 02114, United States

Supporting Information

**ABSTRACT:** The nonenzymatic polymerization of RNA may have enabled copying of functional sequences during the origin of life. Recent progress utilizing 5′-phosphoro-2-aminoimidazole activation has reinvigorated the possibility of using nonenzymatic RNA polymerization for copying arbitrary sequences. However, the reasons why 2-aminoimidazole (AI) is a superior activation group remain unclear. Here we report that the predominant mechanism of polymerization using cytidine-5′-phosphoro-2-aminoimidazolide (Cp*) involves a 2-aminoimidazolium-bridged dinucleotide (Cp*pC) intermediate. To explore the role of this intermediate, we first identify and quantify four reactions involving the synthesis and breakdown of Cp*pC that occur in the absence of the primer−template duplex. We then analyze the dependence of the rate of polymerization on the concentration of the Cp*pC intermediate in the presence and absence of the competitive inhibitor Cp. We also show that the contribution of the monomer Cp* to the polymerization rate is negligible under our primer extension conditions. Finally, we use the experimentally determined rate constants of these reactions to develop a kinetic model that helps explain the changing rate of nonenzymatic RNA polymerization over time. Our model accounts for the concentration of Cp*pC formed by Cp* under primer extension conditions. The model does not completely account for the decline in polymerization rate observed over long times, which indicates that additional important inhibitory processes have not yet been identified. Our results suggest that the superiority of 2-aminoimidazole over the traditional 2-methylimidazole activation is mostly due to the higher level of accumulation of the imidazolium-bridged intermediate under primer extension conditions.

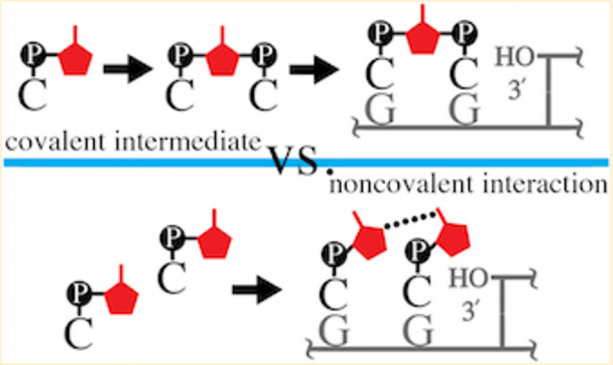


The RNA world hypothesis proposes that early stages of life may have involved the self-replication of RNA oligonucleotides. However, experimental demonstration of RNA self-replication has been extremely difficult, leading some to abandon this hypothesis and suggest alternative scenarios.[1,2] Both the lack of regioselectivity and the limited template generality of nonenzymatic RNA polymerization have been cited as major obstacles to the RNA world. In addition, the prebiotic formation of the canonical RNA nucleosides through glycosylation of ribose is very inefficient, which has raised questions about the availability of RNA in prebiotic environments.[3]

Recent work has revived the hypothesis of a primarily RNA-based foundation to the origin of life. First, the synthesis of both ribonucleotides and amino acids from cyanide and other simple molecular precursors offers a plausible set of prebiotic chemical reactions leading to both RNA and peptides.[4] Second, potential solutions to several steps in the nonenzymatic replication of RNA have been proposed. For example, replacing uridine with 2-thiouridine increases the rate of template-directed nonenzymatic polymerization by increasing the affinity of monomers for the template.[5,6] In addition, the reannealing of a large RNA duplex has been greatly slowed by increased solvent viscosity and RNA secondary structure, allowing information transfer.[7]

Nevertheless, the one-pot synthesis of a functional RNA sequence through template-directed nonenzymatic polymerization has not been achieved and remains a critical goal for establishing a physicochemical approach to primitive genetic inheritance. Recent progress in nonenzymatic template-directed RNA polymerization has utilized RNA monomers combined with downstream oligomers, all activated with a substituted imidazole group on the 5′-phosphate.[8,9] This system iteratively extends the 3′ end of a primer to synthesize a complementary strand, even over difficult mixed-template sequences. Furthermore, the increased length and yield of primer extension reactions have been observed using 2-aminoimidazole instead of 2-methylimidazole activation.[9]

Continued improvement of nonenzymatic RNA polymerization is likely to benefit from a detailed understanding of the chemical mechanism. Our recent report on the kinetics of

Received: August 16, 2017
Revised: October 9, 2017
Published: October 12, 2017




DOI: 10.1021/acs.biochem.7b00792
Biochemistry XXXX, XXX, XXX−XXX

primer extension by 2-methylimidazole-activated monomers suggested that the first step of the mechanism involves the formation of a 2-methylimidazolium-bridged dinucleotide.[10] Upon subsequent binding to the template, this dimer intermediate reacts with the 3′-hydroxyl of the primer, extending it by one nucleotide and releasing an activated monomer as the leaving group. This mechanism contrasts with a previous proposal that two monomers bind the template such that the downstream monomer catalyzes primer extension through noncovalent interactions with the upstream monomer.[8,11] Recent thermodynamic studies have cast doubt on the latter model because the affinity of the monomer in the downstream (+2) position is relatively low.[12] In addition, crystallographic studies of monomers bound to a template revealed a variety of conformations, some of which are not productive for polymerization reactions.[13] In contrast, structural studies of GpppG, a stable analogue of the intermediate, suggest that the imidazolium bridge may help to preorganize the reaction center for polymerization.[14] However, the relative contribution of each of these two mechanisms to the rate of primer extension has not yet been clarified.

Kinetic analysis has been a powerful tool for understanding the reaction mechanism of primer extension systems. For instance, kinetic studies have elucidated the mechanism of 2-MeImpG hydrolysis, a simplified model of template-directed polymerization.[15,16] In addition, two earlier kinetic models identified key determinants of the yield and rate in nonenzymatic RNA polymerization that depend on the particular system studied. Kanavarioti et al.[17,18] account for the synthesis of poly-G catalyzed by poly-C through the quantification of three reactions: monomer hydrolysis, off-template oligomerization, and template-directed primer extension. Also, Kervio et al.[19] have shown that the hydrolysis of 1-hydroxybenzotriazole-activated monomers and competitive inhibition by inactivated monomers are the main limitations for primer extension in that system. However, neither of these models can likely be applied to primer extension by nucleotides activated by 2-aminoimidazole because they do not account for the potential kinetic effects of the imidazolium-bridged dinucleotide intermediate.

Here, we present a kinetic model of nonenzymatic RNA polymerization by cytidine-5′-phosphoro-2-aminoimidazolide (Cp*) (Chart 1). Our results show that the predominant mechanism of polymerization involves a dinucleotide intermediate in which the two 5′-phosphates are bridged by a 2-aminoimidazolium moiety (Cp*pC). To understand the factors that control the concentration of the intermediate, we studied the kinetics of four reactions that affect Cp*pC levels. We first examined the formation of Cp*pC and 2-aminoimidazole (AI) from Cp* under primer extension conditions by $^{31}$P nuclear magnetic resonance (NMR), as well as the reverse process in which AI reacts with Cp*pC to form Cp*. We also measured the rates of hydrolysis of the intermediate Cp*pC and the monomer Cp*. To understand the relationship between the concentration of Cp*pC and nonenzymatic polymerization, we analyzed the rate of primer extension by Cp*pC and competitive inhibition by cytidine 5′-monophosphate (Cp) using Michaelis−Menten kinetics. We combined our empirical rate constants into a kinetic model that relates a series of off-template reactions, including synthesis and decay of Cp*pC, to template-directed primer extension. Our model accounts for the long-term behavior of the off-template reactions and for observations of primer extension rate over the first 2 h. At longer times, additional uncharacterized effects lead to a gradual slowing of the rate of primer extension. Our results suggest that the improved polymerization yield of 2-amino- versus 2-methylimidazole-activated monomers is likely due to the higher level of accumulation of the intermediate under primer extension conditions.

**Chart 1. Chemical Structure and Cartoon Representation of the Molecules Investigated in This Study**

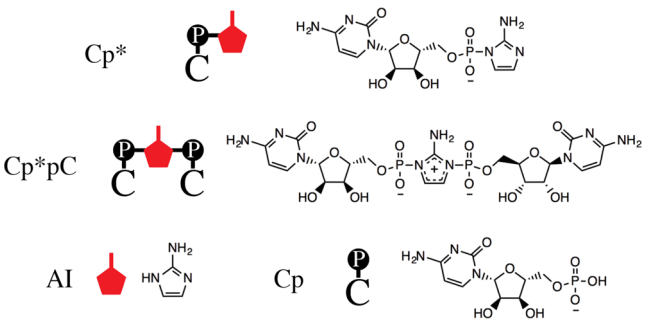


## MATERIALS AND METHODS

All reagents were purchased from Sigma-Aldrich unless specified. 2-Aminoimidazole hemisulfate was purchased from Combi-Blocks, Inc. All other exceptions are specified in our previous report.[10] All syntheses involving the attachment of imidazole to the 5′-phosphate have been previously reported.[9,10]

With the following exceptions, all nonenzymatic primer extension reactions were performed as previously described.[10] For all reactions, the template concentration is 3 $\mu$M and the primer concentration is 2 $\mu$M. Except where noted below, primer extension occurs in 90 mM $MgCl_2$ and 90 mM Tris (pH 8.3−8.4). In Figure 5b, the reactions including 45 mM Cp used 160 mM Tris to improve pH buffering. Also, in Figure 6e, primer extension occurs in 100 mM $MgCl_2$ and 100 mM Tris (pH 8.3−8.4).

All NMR spectra were recorded on a Varian INOVA 400 MHz NMR spectrometer at 25 °C. For all kinetic analyses, samples were prepared in $H_2O$, and a coaxial insert containing $D_2O$ was used for locking. This eliminates possible solvent isotope effects. All peak assignments were confirmed by addition of standards. For characterization, samples were prepared in $D_2O$, and a coaxial insert was not used. Peaks are referenced to internal trimethyl phosphate ($\delta$ 0.00) for $^{31}$P NMR, internal acetone ($\delta$ 30.89) for $^{13}$C NMR, and HOD ($\delta$ 4.79) for $^{1}$H NMR. NMR spectra of Cp*pC characterization are included (Figure S1).

Cp*pC: $^{1}$H NMR (400 MHz) $\delta$ 7.66 (d, $J$ = 7.6 Hz, 1H), 6.96 (m, 1H), 6.03 (d, $J$ = 7.5 Hz, 1H), 5.85 (d, $J$ = 3.2 Hz, 1H), 4.12 (m, 5H); $^{31}$P NMR (161 MHz) $\delta$ −12.84 (s); $^{13}$C NMR (100 MHz) $\delta$ 166.58 (s), 157.90 (s), 150.91 (t, $J$ = 7.1 Hz), 141.62 (s), 116.83 (dd, $J$ = 3.7, 6.7 Hz), 96.77 (s), 90.73 (s), 82.19 (d, $J$ = 8.5 Hz), 74.68 (s), 69.49 (s), 66.16 (d, $J$ = 5.8 Hz); calcd $m/z$ −692.12, observed $m/z$ −692.1.

All NMR spectra were analyzed and quantified using MestReNova software. All kinetic analyses were performed using Microsoft Excel and Prism 7. Parameter fitting of the off-template reactions was performed using code written in R. All values are presented as means ± the standard deviation unless specified otherwise.



DOI: 10.1021/acs.biochem.7b00792
Biochemistry XXXX, XXX, XXX−XXX

## RESULTS AND DISCUSSION

**Cp* Monomers Self-React To Form Cp*pC in Primer Extension Buffer.** We began our analysis of Cp* by determining whether dinucleotide intermediate Cp*pC can form in primer extension buffer (Figure 1a). On the basis of previous studies of 2-MeImpG, we expected that the $Mg^{2+}$ concentration and pH would likely affect our observations.[15] Recent studies of nonenzymatic RNA polymerization have used 50−200 mM $MgCl_2$ and pH 8−9.[8−10] For these experiments, we used 100 mM $MgCl_2$ and 100 mM Tris (pH 8.3−8.4) as the primer extension buffer.

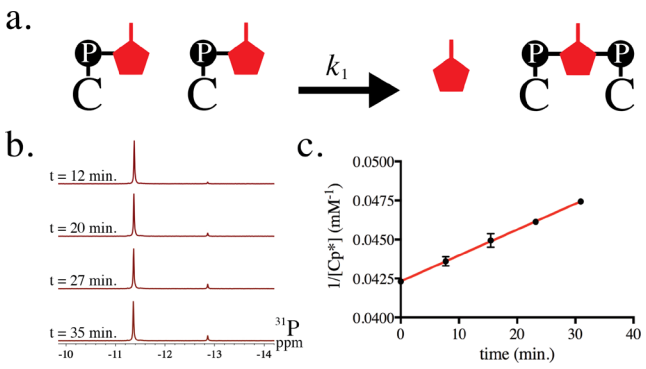


**Figure 1.** Measuring the reaction of two Cp* monomers to form AI and Cp*pC. (a) Schematic of the reaction being measured for calculation of rate constant $k_1$. (b) $^{31}$P NMR spectra of 24 mM Cp* incubated in primer extension buffer over time. Peaks at −11.38 ppm correspond to Cp* and −12.86 ppm to Cp*pC. (c) Analysis of the $^{31}$P NMR spectra at 24 mM Cp* in triplicate by a second-order rate plot. Error bars indicate ±SD ($n$ = 3). The slope is equal to $2k_1$.

Next, we determined rate constant $k_1$ for the reaction of two Cp* monomers to form Cp*pC and AI in primer extension buffer. Samples were prepared in $H_2O$ to avoid potential solvent isotope effects and concentrations measured by integration of $^{31}$P NMR peaks. The formation of AI was not directly observed because AI does not contain a phosphorus atom. We assumed that the observed kinetics would be entirely due to the reaction of two Cp* molecules to form Cp*pC. First, we confirmed that the formation of Cp*pC does indeed follow second-order kinetics by measuring the initial rate of Cp*pC synthesis at four initial concentrations of Cp*. As expected, the initial rate of Cp*pC synthesis increased with the square of the initial concentration of Cp* (Figure S2). Using the 12 experiments with initial Cp* concentrations from 15 to 40 mM, we calculated the second-order rate constant ($k_1$) to be [4.49 ± 0.47 (standard deviation)] × $10^{-3}$ $h^{-1}$ $mM^{-1}$ and to range from 3.65 to 5.22 × $10^{-3}$ $h^{-1}$ $mM^{-1}$ (Figure 1c and Figure S3).

**AI Reacts with Cp*pC To Form Two Molecules of Cp*.** Having determined that intermediate Cp*pC can form in primer extension buffer, we began to consider additional reactions that would affect the concentration of the intermediate during a primer extension experiment. We first examined the reverse of its synthetic reaction, i.e., the nucleophilic attack of AI on Cp*pC to generate two Cp* monomers (Figure 2a). This reaction has not been previously described or measured.

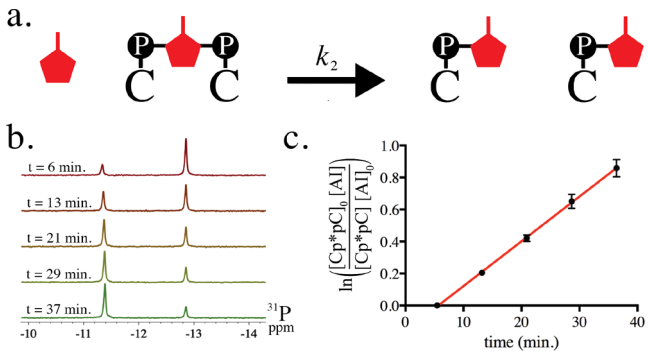


**Figure 2.** Cp*pC reacts with AI to form two molecules of Cp*. (a) Schematic of the reaction measured to determine $k_2$. (b) $^{31}$P NMR spectra of 5 mM Cp*pC and 11.5 mM AI incubated in primer extension buffer. The peaks at −11.41 ppm correspond to monomer Cp* and −12.86 ppm to dinucleotide intermediate Cp*pC. (c) Analysis of the reaction between 5 mM Cp*pC and 11.5 mM AI in a second-order kinetic plot. In the plot, $k_2$ is equal to the slope divided by $[AI]_0 - [Cp*pC]_0$. Error bars indicate ±SD ($n$ = 3).

To follow the reaction of AI with Cp*pC, 11.5 mM AI was incubated with 5 mM Cp*pC in primer extension buffer, and the progress of the reaction was monitored by $^{31}$P NMR spectroscopy (Figure 2b). We observed that the magnitude of the peak for Cp*pC rapidly decreased and that the magnitude of the peak for Cp* increased over time. In addition, the concentration of Cp did not significantly change during the course of the reaction. This indicates that the increase in the level of Cp* is not due to hydrolysis of Cp*pC. Instead, these results indicate that AI reacts with Cp*pC to form two molecules of Cp*.

We measured the rate of the reaction between AI and Cp*pC at five different concentrations to determine the reaction order. On the basis of the reaction order, the kinetics should be overall second-order for this reaction, with first-order for both AI and Cp*pC. A reaction order of ∼0.8 was determined for both AI and Cp*pC (Figure S4). We suspect that the empirical determinations of the reaction order might be slight underestimations because of the technical difficulty of measuring the fast rate of the reaction. The 15 experiments with varying concentrations of 5.75−17.25 mM AI and 2.5−7.5 mM Cp*pC were analyzed using second-order kinetic plots to calculate a $k_2$ of 0.238 ± 0.020 (SD) $h^{-1}$ $mM^{-1}$ with a range of 0.190−0.271 $h^{-1}$ $mM^{-1}$ (Figure 2c and Figure S5).

**Cp*pC Hydrolyzes to Cp* and Cp.** In addition to reacting with AI, we expected that Cp*pC would also decay through hydrolysis to form Cp and Cp* (Figure 3a). This reaction has been previously observed for the 2-methylimidazolium-bridged dinucleotide.[10] To measure this reaction, $^{31}$P NMR spectra of 5 mM Cp*pC in primer extension buffer were


DOI: 10.1021/acs.biochem.7b00792
Biochemistry XXXX, XXX, XXX−XXX

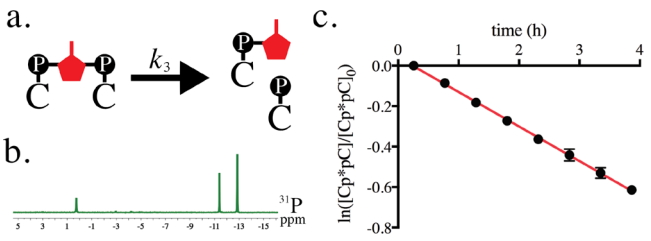


**Figure 3.** Intermediate Cp*pC hydrolyzes to Cp* and Cp. (a) Schematic of the reaction measured to determine $k_3$. (b) $^{31}$P NMR spectrum of 5 mM Cp*pC incubated in primer extension buffer for 3.9 h. The peak at 0.28 ppm corresponds to Cp, that at −11.41 ppm to Cp*, and that at −12.86 ppm to Cp*pC. (c) Quantification of hydrolysis in a first-order kinetic plot. The negative slope is equal to $k_3$ = 0.171 ± 0.006 h$^{-1}$. Error bars indicate ±SD ($n$ = 3).

recorded every 31 min for 4.1 h (Figure 3b). In the absence of free AI, the observed changes in concentration during this time frame should be entirely due to hydrolysis of Cp*pC. As expected, the intermediate decayed to approximately equal amounts of Cp and Cp*, consistent with hydrolysis of Cp*pC (Figure S6). We calculated a pseudo-first-order rate constant of intermediate hydrolysis [$k_3$ = 0.171 ± 0.006 h$^{-1}$ (Figure 3c)]. This value corresponds to a half-life of 4.06 ± 0.15 h.

As a comparison to the traditional 2-methylimidazole activation, the hydrolysis rate of the 2-methylimidazolium-bridged dicytidine intermediate was also measured under similar reaction conditions (Figure S7). We used a partially purified 2-methylimidazolium intermediate as described in our previous report.[10] The observed rate constant of hydrolysis for the 2-methylimidazolium intermediate was determined to be 4.40 ± 0.07 h$^{-1}$. This value is 26 times higher than the hydrolysis rate constant of 2-aminoimidazolium Cp*pC, indicating that 2-aminoimidazolium Cp*pC is much more stable than the 2-methylimidazolium intermediate.

**The Cp* Monomer Slowly Hydrolyzes to Cp and AI.** We also measured the rate of hydrolysis of Cp* in primer extension buffer (Figure 4a). Measuring the hydrolysis rate of

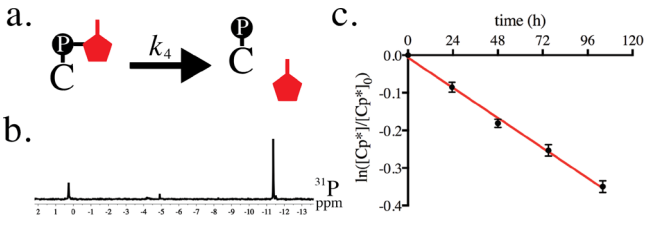


**Figure 4.** Monomer Cp* decays slowly to Cp and AI. (a) Schematic of the reaction measured to determine $k_4$. (b) $^{31}$P NMR spectrum of 5 mM Cp* and 20 mM AI incubated in primer extension buffer for 72 h. The peak at 0.29 ppm corresponds to Cp and that at −11.39 ppm to Cp*. The peak at −4.92 ppm corresponds to cyclic cytidine 3′,5′-monophosphate as verified by spike-in. (c) Hydrolysis of 5 mM Cp* in 40 mM AI quantified by $^{31}$P NMR spectra in a first-order rate plot. The negative slope is equal to $k_4$ = (3.33 ± 0.03) × 10$^{-3}$ h$^{-1}$. Error bars indicate ±SD ($n$ = 3).

Cp* was complex because Cp* also self-reacts to form Cp*pC (Figure 1), which can then hydrolyze to Cp, the product of Cp* hydrolysis. To minimize the concentration of Cp*pC, the hydrolysis of Cp* in primer extension buffer was measured at a series of concentrations of AI. We hypothesized that the excess AI would react with Cp*pC to form two Cp* molecules (Figure 2), thereby reducing the Cp*pC concentration without affecting Cp* hydrolysis.

We began our analysis of the hydrolysis of Cp* by recording $^{31}$P NMR spectra of 5 mM Cp* and 20 mM AI over 5 days. Cp* gradually decayed into Cp as well as trace amounts of other products that were detected on the third day (Figure 4b). A peak corresponding to Cp*pC was not observed, suggesting that Cp formed directly by hydrolysis of Cp*. In the presence of 20 mM AI, we calculated the observed Cp* hydrolysis rate constant [$k_4$ = (4.04 ± 0.16) × 10$^{-3}$ h$^{-1}$].

Given that $k_3$ is ∼40 times greater than $k_4$, our results could easily be affected by trace levels of Cp*pC. We repeated our experiment using 40 mM AI and 5 mM Cp* in primer extension buffer. This time we observed that $k_4$ = (3.33 ± 0.03) × 10$^{-3}$ h$^{-1}$ (Figure 4c), suggesting that our previous results overestimated $k_4$ because of trace formation of Cp*pC. Again, our experiments were repeated using 60 mM AI. However, a precipitate was observed on the third day of the experiment, and these data were not analyzed. Overall, these results place an upper limit on the value of $k_4$ and suggest that the half-life of Cp* is >8.7 days because of hydrolysis in primer extension buffer. In addition, we observed that the rate constant of 2-MeImpC hydrolysis equals (2.93 ± 0.26) × 10$^{-3}$ h$^{-1}$ under comparable conditions (Figure S8).

**Cp*pC Is a Substrate for Primer Extension.** Because Cp*pC both forms and decays in primer extension buffer, we began investigating how the concentration of Cp*pC affects the rate of primer extension. This relationship can be approximated through Michaelis−Menten kinetics because of the separate binding and reaction steps that occur on the primer−template complex. The primer−template complex is present at very low concentrations relative to those of substrates, which show saturation binding.[19−21] In addition, Michaelis−Menten kinetics offers a framework for studying the effect of competitive inhibition on the polymerization rate (Figure 5a).

We determined the rate of primer extension using five concentrations of Cp*pC from 0.5 to 20 mM. We observed that the pseudo-first-order rate constant of polymerization during the first 3 min, $k_{obs}$, increased with the concentration of

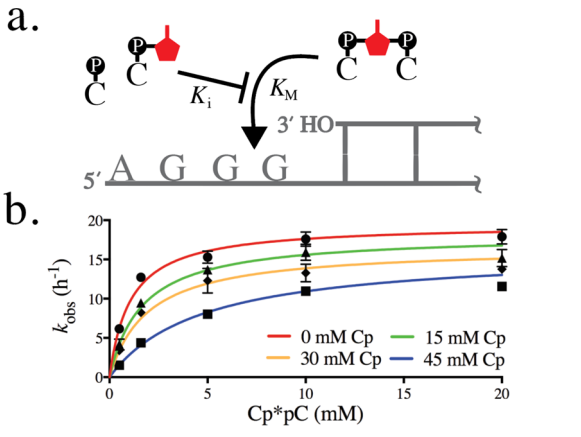


**Figure 5.** Cp competitively inhibits primer extension by Cp*pC. (a) During the primer extension reaction, Cp*pC binds the template with an affinity related to the $K_M$. The Cp and Cp* monomers also bind the template and competitively inhibit the primer extension reaction. (b) Michaelis−Menten plot of Cp*pC with 0−45 mM Cp. Lines represent the Michaelis−Menten equation evaluated with empirical determinations of $k_{obsmax}$ and effective $K_M$. Error bars indicate ±SD ($n$ = 3).



DOI: 10.1021/acs.biochem.7b00792
Biochemistry XXXX, XXX, XXX−XXX

the intermediate (Figure S9). $k_{obs}$ plateaus at Cp*pC concentrations above 5 mM, suggesting that the template becomes saturated by Cp*pC binding (Figure 5b, red line). We analyzed these data using a double-reciprocal plot and substituted $V_{max}$ with $k_{obsmax}$ for the purpose of comparison. For primer extension by Cp*pC in the absence of competitive inhibition, we observed that $k_{obsmax}$ = 19.5 ± 2.1 $h^{-1}$ and $K_M$ = 1.06 ± 0.12 mM.

Having determined that Cp*pC is a substrate of the primer extension reaction, we next analyzed how the monomer competitively inhibits primer extension by Cp*pC. We repeated our Michaelis−Menten analysis of Cp*pC in the presence of 15−45 mM Cp and observed increasingly lower rates for this set of reactions compared to the set with 0 mM Cp (Figure 5b). Overall, this set of data is consistent with competitive inhibition as analyzed by a double-reciprocal plot (Figure S10). As expected, the effective $K_M$ increases with Cp concentration. On the basis of these values, we calculated that the $K_i$ of Cp inhibition of primer extension by Cp*pC is 24.7 ± 11.6 mM. This value agrees with the $K_d$ of 15−19 mM of Cp measured for a different RNA duplex.[20] In addition, this value is consistent with the $K_d$ of 19 mM for Cp and the $K_d$ of 27 mM for 2-MeImpC previously determined for an RNA hairpin.[21]

We also note that our calculated $k_{obsmax}$ slightly decreases at higher concentrations of Cp, suggesting possible mixed inhibition. However, we cannot fully exclude potential nonspecific effects of adding Cp, such as changing the ionic strength of the primer extension reaction. In total, the data indicate that $k_{obsmax}$ = 17.6 ± 1.6 $h^{-1}$, which is within error of our values obtained with both 0 mM Cp and 45 mM Cp.

**Cp* Does Not Discernibly Contribute to the Primer Extension Rate.** We next sought to determine the rate of primer extension by Cp* directly reacting with the primer. The interpretation of these experiments is complicated by the fact that Cp* forms Cp*pC under primer extension conditions (Figure 1). However, we have quantified Cp*pC formation and the rate of primer extension by Cp*pC via competitive inhibition (Figure 5). Therefore, we can account for the rate of primer extension due to Cp*pC and then determine the rate due to Cp*, including possible noncovalent interactions between template-bound Cp*. We decided on a final Cp* concentration of 30 mM for these experiments to be above the $K_d$ of the monomer, but not too high to limit Cp*pC formation at short time intervals.

The primer extension assay was initiated by adding a 45 mM Cp* stock at pH 9.6 to a reaction mix for final concentrations of 30 mM Cp*, 90 mM Tris, 90 mM $MgCl_2$, 2 μM primer, and 3 μM template, identical to our analysis of Cp*pC. We observed the reaction over the first 8 min, during which time the reaction rate noticeably increased, likely because of the formation of Cp*pC (Figure 6a). A similar phenomenon has been reported for primer extension by 2-MeImpG.[10] Because of this "speed-up" effect, the calculated rate of primer extension is only approximated by pseudo-first-order kinetic plots. For the first 3 min of the primer extension time course, we observed that the initial rate constant of primer extension $k_{obs}$ = 0.93 ± 0.11 $h^{-1}$. In comparison, $k_{obs}$ = 2.6 ± 0.5 $h^{-1}$ for the last 3 min of this time course.

To account for the primer extension rate due to Cp*pC, we first calculated the concentration of Cp*pC using the previously determined $k_1$. On the basis of this value, we expect an average concentration of 65 ± 3 μM Cp*pC over the first 3 min of the primer extension reaction. By using the $K_M$ and $K_i$ values previously obtained and propagating the errors, we approximate that the $k_{obs}$ due to Cp*pC is ≈0.47 ± 0.13 $h^{-1}$. This calculation suggests that part of the observed rate may be due to Cp* directly extending the primer. However, a low initial concentration of Cp*pC in our Cp* stock at pH 9.6 could explain the discrepancy. We repeated our calculations for the 6−8 min interval and computed a $k_{obs}$ of 2.0 ± 0.5 $h^{-1}$, which is within error of the observed value.

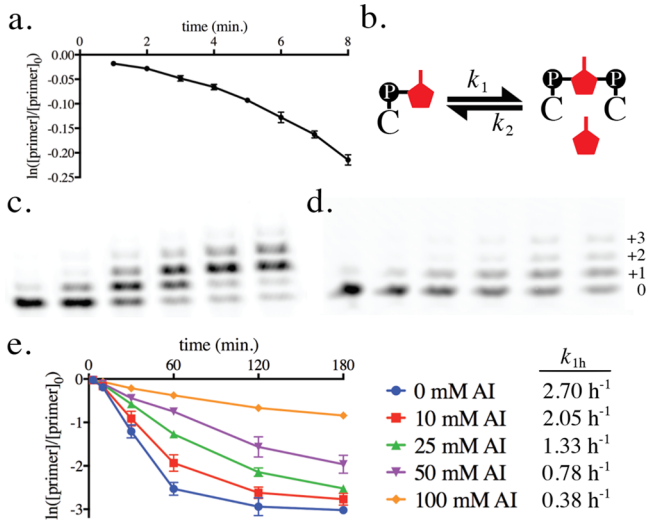


**Figure 6.** Primer extension in the presence of Cp* is largely due to the formation of Cp*pC. (a) Pseudo-first-order plot of primer extension initiated by the Cp* stock at pH 9.6. (b) Schematic illustrating that addition of AI favors Cp* at the expense of Cp*pC. (c) Gel image of nonenzymatic RNA primer extension with 20 mM Cp* and no additional AI. Samples are at 3, 10, 30, 60, 120, and 180 min. (d) Gel image of nonenzymatic RNA primer extension with 20 mM Cp* and 100 mM AI. (e) Pseudo-first-order plot of nonenzymatic RNA primer extension with various concentrations of AI. The observed values of rate constant $k_{1h}$ are recorded in the key. Error bars indicate ±SD ($n$ = 3).

We sought another approach to directly measure primer extension by Cp* by reducing the Cp*pC concentration. Previously, excess AI was used to decrease the concentration of Cp*pC in Cp* solutions when studying hydrolysis (Figures 4 and 6b). We adopted a similar approach by adding 0−100 mM AI to a series of primer extension reaction mixtures containing a final Cp* concentration of 20 mM. Because of the low rates, we observed the primer extension reactions for 3 h. In addition, we used 100 mM $MgCl_2$ and 100 mM Tris.

Addition of AI greatly inhibited the primer extension reaction (Figure 6c,d). For this set of experiments, we compared a pseudo-first-order rate constant calculated from the first hour of the primer extension reaction, $k_{1h}$. For 0 mM AI, we observed that $k_{1h}$ = 2.70 $h^{-1}$. At 100 mM AI, we observed that $k_{1h}$ = 0.38 $h^{-1}$. Notably, the rate markedly declines between 50 and 100 mM AI, suggesting that our observed rate constant is an upper limit to the polymerization rate of Cp*.

From these data, we extrapolated the primer extension rate to infinitely high concentrations of AI, or when the Cp*pC concentration is zero. For the purpose of this calculation, we assumed that Cp* is in equilibrium with Cp*pC and AI (Figure 6b). To estimate the equilibrium constant, we noted that $K_{eq}$ = $k_1/k_2$ = 0.019 ± 0.004 (Figure S11). Because $K_{eq}$ = [Cp*pC][AI][Cp*]$^{-2}$, [AI] is reciprocal to [Cp*pC], and this equation can be used to approximate the concentration of


DOI: 10.1021/acs.biochem.7b00792
Biochemistry XXXX, XXX, XXX−XXX

Cp*pC when [AI] is varied. The $k_{1h}$ values were plotted versus the approximated [Cp*pC] values in a Michaelis–Menten plot (Figure S12). We then analyzed this plot using nonlinear regression to a Michaelis–Menten equation modified with a constant term to represent the possible reaction rate due to 20 mM Cp*. We observed that the *y*-intercept, when [Cp*pC] is zero, is equal to $-0.286 \pm 0.159$ $h^{-1}$ standard error. This negative value of $k_{1h}$ is likely due to an overestimation of [Cp*pC] from the $K_{eq}$ value, because Cp*pC also hydrolyzes. However, our analysis suggests that the contribution of Cp* to the primer extension rate is indistinguishable from zero under these conditions.

**Kinetic Modeling of the Primer Extension Reaction.** We sought to combine our kinetic data into a kinetic model to develop and test our understanding of the primer extension reaction. The model needed to explain both the concentration of the intermediate formed over time under primer extension conditions and how this affects the rate of polymerization. We reasoned that solutions of Cp* would undergo a series of off-template reactions involving Cp*pC, AI, and Cp (Scheme 1).

**Scheme 1. Kinetic Model of Primer Extension by Cp*[a]**

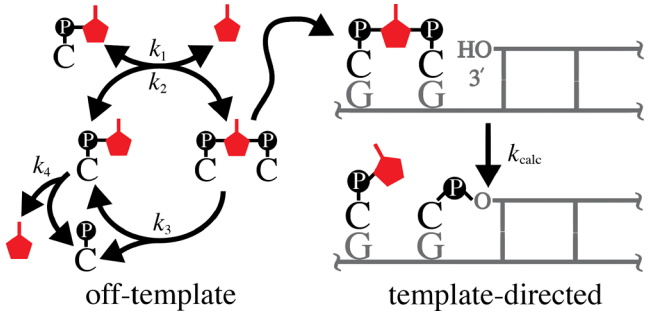


[a]On the left, the off-template reactions form and destroy Cp* and Cp*pC. Cp is formed as a hydrolysis product. On the right, the primer is extended by only Cp*pC. Primer extension is also competitively inhibited by Cp* and Cp.

Only intermediate Cp*pC binds the template and subsequently reacts with the primer. As observed in our analysis of inhibition by AI, the reaction of Cp* with the primer is too slow to significantly affect the rate of polymerization (Figure 6). Finally, we assume that the concentrations of AI, Cp, Cp*, and Cp*pC are not greatly affected by the primer–template duplex on short time scales.

We modeled the four off-template reactions using four kinetic rate equations to describe how the concentration of each molecule will change over time.

$$d[Cp^*]/dt = -2k_1[Cp^*]^2 + 2k_2[Cp^*pC][AI] + k_3[Cp^*pC] - k_4[Cp^*] \quad (1)$$

$$d[Cp^*pC]/dt = k_1[Cp^*]^2 - k_2[Cp^*pC][AI] - k_3[Cp^*pC] \quad (2)$$

$$d[Cp]/dt = k_3[Cp^*pC] + k_4[Cp^*] \quad (3)$$

$$d[AI]/dt = k_1[Cp^*]^2 - k_2[Cp^*pC][AI] + k_4[Cp^*] \quad (4)$$

In these equations, rate constants $k_1$–$k_4$ correspond to the reactions studied by $^{31}$P NMR (Figures 1–4 and Table 1). By iteratively solving these equations following initial conditions, we can model the concentrations of all four molecules over time.

**Table 1. Off-Template Reaction Rate Constants ± SD Observed Experimentally (Figures 1–4) or Computationally Fit to 24 mM Cp* Solutions (Figure 7)**

| | observed | fitted |
|---|---|---|
| $k_1$ ($h^{-1}$ $mM^{-1}$) | $(4.49 \pm 0.47) \times 10^{-3}$ | $(4.55 \pm 0.48) \times 10^{-3}$ |
| $k_2$ ($h^{-1}$ $mM^{-1}$) | $0.238 \pm 0.020$ | $0.183 \pm 0.026$ |
| $k_3$ ($h^{-1}$) | $0.171 \pm 0.006$ | $0.167 \pm 0.012$ |
| $k_4$ ($h^{-1}$) | $(3.33 \pm 0.03) \times 10^{-3}$ | $(2.11 \pm 0.84) \times 10^{-3}$ |

We modeled the rate of the primer extension reaction based on our Michaelis–Menten kinetic analysis of primer extension by Cp*pC (Figure 5). The rate constant of polymerization can be calculated using the relationship

$$k_{calc} = k_{obsmax}[Cp^*pC]/(K_{eff} + [Cp^*pC]) \quad (5)$$

$$K_{eff} = K_M[1 + ([Cp] + [Cp^*])/K_i] \quad (6)$$

where $k_{obsmax}$, $K_M$, and $K_i$ are empirically determined constants (Figure 5). These equations combine the Michaelis–Menten equation with competitive inhibition by the monomers, Cp and Cp*. Under our reaction conditions, both Cp and Cp* are assumed to bind the template with approximately equal affinity to competitively inhibit primer extension. Using the calculated concentrations of Cp, Cp*, and Cp*pC (eqs 1–4) to evaluate $k_{calc}$ (eqs 5and 6), we can model how the polymerization rate of nonenzymatic primer extension changes over time due to the off-template reactions.

**Analyzing Long-Term Behavior of Off-Template Reactions with the Kinetic Model.** We first tested our kinetic model of the off-template reactions against experimental data obtained by $^{31}$P NMR (Figure 7). Beginning with 24 mM Cp* in primer extension buffer, we observed the concentrations of Cp, Cp*, and Cp*pC every 7 min and 44 s for 12.5 h.

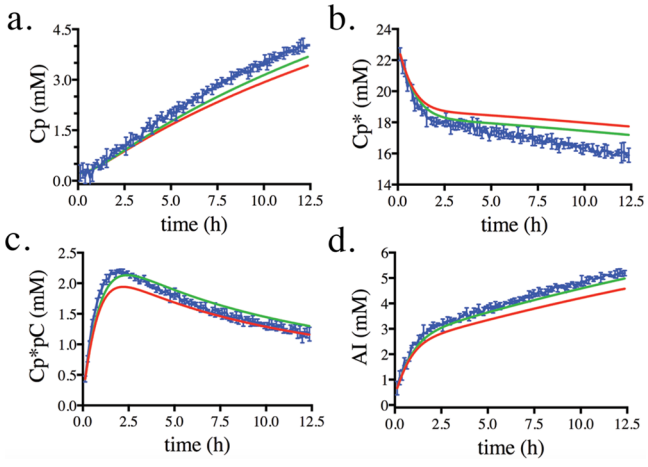


**Figure 7.** Kinetic model describing the long-term behavior of off-template reactions in 24 mM Cp* solutions in primer extension buffer. Concentrations over time for experimentally observed (blue), empirical model (red), and fitted model (green) are presented for (a) Cp, (b) Cp*, (c) Cp*pC, and (d) AI. Concentrations were experimentally determined using $^{31}$P NMR. Modeled concentrations were iteratively calculated using eqs 1–4 and the rate constants listed in Table 1.



DOI: 10.1021/acs.biochem.7b00792
*Biochemistry* XXXX, XXX, XXX–XXX

Because AI cannot be observed by $^{31}$P NMR, we inferred that the concentration of AI is equal to the concentration of Cp plus Cp*pC.

Our experimental observations of off-template reactions displayed dynamic changes in concentration for some of the molecules. For Cp, the concentration steadily increased over time from 0.2 to 4.0 mM over 12.5 h (Figure 7a, blue line). In contrast, the concentration of Cp* rapidly decreased from 22.4 to 18.0 mM over the first 2 h and then slowly decreased to 15.9 mM over the next 10.5 h (Figure 7b, blue line). For Cp*pC, we observed a sharp increase over the first 2 h from 0.4 to 2.2 mM (Figure 7c, blue line). At this peak concentration, Cp*pC accounts for 18% of the cytidine present in the mixture. Over the next 10.5 h, the concentration of Cp*pC gradually decreases to 1.2 mM. Finally, the AI concentration was inferred to sharply increase during the first 2 h from 0.7 to 3.1 mM and then gradually increase to 5.2 mM by the end of the NMR series (Figure 7d, blue line). In addition, we also observed four peaks from trace products (Figure S13).

We compared these data to our kinetic model initialized with the concentrations observed in the first spectrum of the NMR series and a step size of 1 min for d$t$ in our calculations. Overall, we observed similar trends between our model and the experimental observations of the four molecules (Figure 7, red lines). For Cp*, Cp*pC, and AI, the model predicts a 2 h initial phase of rapid concentration change, followed by a second phase of gradual changes. However, there are important discrepancies between the model and the experimental data. Most notable is the 14% difference between the calculated and observed concentrations of Cp at the end of the time course (Figure 7a). This may be due in part to the 12% underestimation of Cp*pC at its peak concentration near 2 h (Figure 7c). In addition, a 1.9 mM difference develops between the model and the observed concentration of Cp* (Figure 7b). Part of this discrepancy is likely due to the formation of trace materials that amount to ∼1.8 mM by 12.5 h. Future studies of the off-template reactions should account for the formation of these trace materials.

Given the differences between the model and the observed concentrations, we computationally fit the off-template $k$ values to this experimental data set. Our approach randomly varied $k$ values within ±20% for 100 iterations and then computed the concentrations of all four molecules for 12.5 h. The $k$ values were kept if they simultaneously improved the square of normalized residuals for all of the molecules. As our input $k$ values for the first iteration, we used the experimentally determined $k$ values randomly multiplied or divided by up to 2 times.

We repeated this calculation 100 times and then averaged the fitted $k$ parameters (Table 1). As expected, the fitted $k$ values improve our agreement between the kinetic model and experimental observations (Figure 7, green lines). In general, the fitted $k$ values agree with our experimental determinations of $k_1$ and $k_3$ but significantly differ from our determinations of $k_2$ and $k_4$ (Table 1). Notably, this analysis suggests that we systematically overestimated rate constant $k_2$, which caused our empirical model to underestimate the level of Cp*pC and subsequently underestimate the levels of Cp and AI.

**The Kinetic Model Explains the Rate of Primer Extension at Early Times.** Next, we compared our predicted $k_{calc}$ against the experimentally determined $k_{obs}$ of primer extension reactions over time. To determine how the rate of polymerization changes over 10 h, we incubated 24 mM Cp* in primer extension buffer and periodically removed aliquots to initiate primer extension reactions and determine $k_{obs}$. After addition of Cp*, the primer extension mixture contains 90 mM $MgCl_2$ and 90 mM Tris, which is identical to the conditions of our $K_M$ determination (Figure 5).

We observed that the change in the $k_{obs}$ of primer extension displayed two stages (Figure 8a). In the first 2 h, the $k_{obs}$ of

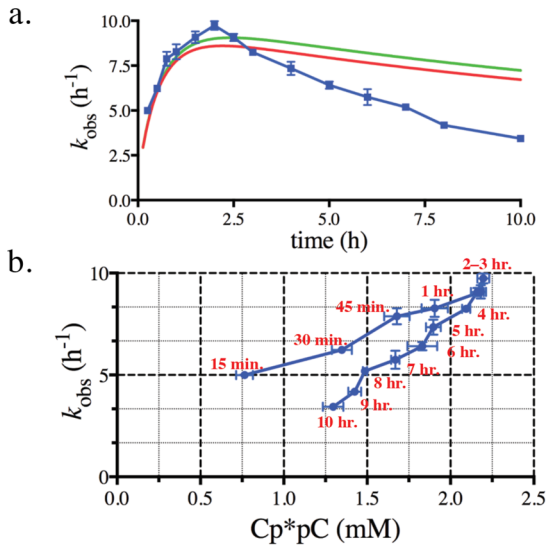


**Figure 8.** $k_{obs}$ drifts lower than $k_{calc}$ over long-term primer extension experiments. (a) A 24 mM Cp* solution incubated in primer extension buffer is used to initiate primer extension reactions at various times to obtain $k_{obs}$ (blue). $k_{calc}$ is obtained by evaluating eqs 5 and 6 with concentrations calculated using the empirically determined (red) or computationally fit (green) rate constants of the off-template reactions. (b) Experimentally determined $k_{obs}$ values of primer extension are plotted vs the concentration of Cp*pC observed by $^{31}$P NMR.

primer extension increases from 5.0 to 9.7 h$^{-1}$. Subsequently, $k_{obs}$ steadily declines to 3.4 h$^{-1}$ after incubation for 10 h in primer extension buffer. On the basis of our model using either the empirical or fitted off-template parameters listed in Table 1, the change in $k_{calc}$ also displayed two stages over 10 h. For the fitted parameters, $k_{calc}$ increases during the first 2 h from 2.9 to 9.0 h$^{-1}$ and then gradually decreases to 7.2 h$^{-1}$ by the end of the time course (Figure 8a, green line). By comparing $k_{calc}$ with $k_{obs}$, we observed that this model agrees with observation for the first 2 h but subsequently overestimates the polymerization rate for the next 8 h. The difference between $k_{calc}$ and $k_{obs}$ grows over time and cannot be explained by a difference between observed and calculated concentrations. These results indicate that the decline in $k_{obs}$ is not fully explained by Cp*pC polymerization and competitive inhibition by monomers Cp and Cp*.

To better understand the reasons why the model does not fully explain the rate of primer extension, we analyzed a plot of $k_{obs}$ versus the concentration of Cp*pC observed by $^{31}$P NMR (Figure 8b). This plot was obtained by combining the data from Figures 7c and 8a and eliminating the time variable. We observed a positive correlation between $k_{obs}$ and the concentration of the intermediate (Pearson $r$ = 0.836, and two-tailed $p$ < 0.0002), suggesting that the concentration of Cp*pC is a key factor that determines the polymerization rate. In addition, we noticed that the later time points generally


DOI: 10.1021/acs.biochem.7b00792
Biochemistry XXXX, XXX, XXX−XXX

displayed a value for $k_{obs}$ lower than those of earlier time points. For instance, the observed concentration of Cp*pC at both 30 min and 10 h is 1.3 mM. However, $k_{obs}$ = 6.2 $h^{-1}$ at 30 min, and $k_{obs}$ = 3.4 $h^{-1}$ at 10 h. These results suggest that an additional factor is changing over time to decrease the rate of primer extension. We hypothesize that trace amounts of potent inhibitors, possibly short oligomers, may accumulate over time. Alternatively, hydrolysis products AI and Cp might inhibit primer extension in ways not represented by our analysis. Future improvement of the kinetic model should identify and analyze the cause of decreased rates in long-term experiments.

## CONCLUSIONS

We have provided a kinetic model that recapitulates several features of the primer extension reaction over time and establishes that the predominant mechanism of nonenzymatic RNA polymerization of cytidine-5′-phosphoro-2-aminoimidazolide involves reaction of the primer with Cp*pC. Although we cannot entirely exclude the traditional mechanism of a nucleophilic attack from the primer on Cp*, the contribution of this proposed mechanism to the reaction rate is negligible (<0.4 $h^{-1}$) under these conditions. This is likely due to the enhanced reactivity of Cp*pC relative to Cp*, as well as the higher affinity of the dinucleotide intermediate for the template. In addition, the alternative mechanism of a downstream monomer mediating a noncovalent "leaving group−leaving group" interaction under these conditions is unlikely based upon measured binding affinities and analogue studies.[12,13]

Although this study clarifies the chemical mechanism of polymerization solely using monomers, the effect of downstream oligomers on the mechanism remains to be investigated. Possibly, noncovalent interactions occur using a stably bound downstream oligomer activated with AI. In addition, we have yet to explicitly investigate the catalysis of Cp*pC formation by a complementary template. Previous reports indicate that complementary oligonucleotides act as a template for the reaction between 2-methylimidazole-activated monomers and ribonucleotide 5′-monophosphates to form dinucleotide 5′,5′-pyrophosphates.[22,23] This work suggests that two template-bound Cp* might locally react to form Cp*pC and then polymerize.[24]

The differences between the kinetic model and the experimental observations identify gaps in our understanding of nonenzymatic RNA polymerization. First, the kinetic model does not include the formation of the trace materials observed after extended incubation in primer extension buffer. Second, the rate of polymerization decreases more quickly than our model predicts. This leads us to speculate that these trace compounds might be the inhibitors that explain why the polymerization rate decreases more quickly than expected. However, we note that the potential formation of inhibitors may be a peculiarity of the specific reaction system we have studied. Future extensions of the kinetic model should address additional, more complex systems, including multiple monomers and mixed-template sequences.

Lastly, our results address the reasons why 5′-phosphoro-2-aminoimidazole activation outperforms that of 2-methylimidazole. When we incubated 24 mM 2-MeImpC in primer extension buffer, we did not observe detectable levels of the corresponding 2-methylimidazolium-bridged dinucleotide by $^{31}$P NMR (Figure S14). Because it is readily detectable at lower pH, we hypothesize that it is present at low concentrations.[10] We suspect two reasons for the accumulation of the 2-aminoimidazolium Cp*pC. First, the formation of the intermediate is pH-dependent and is optimal when pH = p$K_a$.[10] The higher p$K_a$ of the 2-aminoimidazole group is more favorable than 2-methylimidazole for formation of the intermediate at pH 8.3−8.4.[9] Second, the increased stability of the 2-aminoimidazolium Cp*pC relative to the 2-methylimidazolium dinucleotide also favors accumulation of this molecule under primer extension conditions (Figure 3 and Figure S7). We note that the 2-methylimidazolium intermediate was too reactive to effectively purify in our previous study,[10] but we were readily able to synthesize the 2-aminoimidazolium Cp*pC with >90% purity in this work. Unexpectedly, the hydrolysis rates of the 2-MeImpC and the 2-amino Cp* were very similar when free imidazole was used to limit formation of the intermediate (Figure 4 and Figure S8). This observation differs from a previous result suggesting that the 2-amino monomer hydrolyzes twice as fast as the 2-methyl monomer under primer extension conditions.[9] Because of the comparable stabilities of these monomers, we suspect that the nucleophilicity of the imidazole group also plays an important role in the strongly enhanced reaction rate of 2-aminoimidazole-activated monomers. Continuing investigations of the reaction mechanism will help to clarify the reasons for the superiority of 2-aminoimidazole and identify the reaction pathways that will need to be optimized to further improve nonenzymatic RNA polymerization.

## ASSOCIATED CONTENT

### Supporting Information

The Supporting Information is available free of charge on the ACS Publications website at DOI: 10.1021/acs.biochem.7b00792.

Supplementary Figures S1−S14 (PDF)

## AUTHOR INFORMATION


### Corresponding Author

*E-mail: szostak@molbio.mgh.harvard.edu.

### ORCID

Travis Walton: 0000-0001-6812-1579

Jack W. Szostak: 0000-0003-4131-1203


### Author Contributions

The manuscript was written through contributions of both authors. Both authors have given approval to the final version of the manuscript. T.W. designed and performed the experiments. J.W.S. designed the experiments.


### Funding

J.W.S. is an Investigator of the Howard Hughes Medical Institute. This work was supported in part by National Science Foundation Grant CHE-1607034 to J.W.S. and a grant (290363) from the Simons Foundation to J.W.S.


### Notes

The authors declare no competing financial interest.

## ACKNOWLEDGMENTS


The authors acknowledge the helpful advice and assistance of Derek O'Flaherty, Chun Pong Tam, and Lydia Pazienza.


## ABBREVIATIONS

2-MeImpC, cytidine-5′-phosphoro-2-methylimidazolide; 2-MeImpG, guanosine-5′-phosphoro-2-methylimidazolide; AI, 2-aminoimidazole; Cp, cytidine 5′-monophosphate; Cp*,



DOI: 10.1021/acs.biochem.7b00792
Biochemistry XXXX, XXX, XXX−XXX

cytidine-5′-phosphoro-2-aminoimidazolide; Cp*pC, 1,3-di-(cytidine-5′-phosphoro)-2-aminoimidazolium; SD, standard deviation.

## REFERENCES


(1) Robertson, M. P., and Joyce, G. F. (2012) The origins of the RNA world. *Cold Spring Harbor Perspect. Biol. 4*, a003608.

(2) Hud, N. V., Cafferty, B. J., Krishnamurthy, R., and Williams, L. D. (2013) The origin of RNA and "my grandfather's axe". *Chem. Biol. 20*, 466−474.

(3) Orgel, L. E. (2004) Prebiotic chemistry and the origin of the RNA world. *Crit. Rev. Biochem. Mol. Biol. 39*, 99−123.

(4) Patel, B. H., Percivalle, C., Ritson, D. J., Duffy, C. D., and Sutherland, J. D. (2015) Common origins of RNA, protein and lipid precursors in a cyanosulfidic protometabolism. *Nat. Chem. 7*, 301−307.

(5) Heuberger, B. D., Pal, A., Del Frate, F., Topkar, V. V., and Szostak, J. W. (2015) Replacing uridine with 2-thiouridine enhances the rate and fidelity of nonenzymatic RNA primer extension. *J. Am. Chem. Soc. 137*, 2769−2775.

(6) Larsen, A. T., Fahrenbach, A. C., Sheng, J., Pian, J., and Szostak, J. W. (2015) Thermodynamic insights into 2-thiouridine-enhanced RNA hybridization. *Nucleic Acids Res. 43*, 7675−7687.

(7) He, C., Gállego, I., Laughlin, B., Grover, M. A., and Hud, N. V. (2017) A viscous solvent enables information transfer from gene-length nucleic acids in a model prebiotic replication cycle,. *Nat. Chem. 9*, 318−324.

(8) Prywes, N., Blain, J. C., Del Frate, F., and Szostak, J. W. (2016) Nonenzymatic copying of RNA templates containing all four letters is catalyzed by activated oligonucleotides. *eLife 5*, e17756.

(9) Li, L., Prywes, N., Tam, C. P., O'Flaherty, D. K., Lelyveld, V. S., Izgu, E. C., Pal, A., and Szostak, J. W. (2017) Enhanced nonenzymatic RNA copying with 2-aminoimidazole activated nucleotides. *J. Am. Chem. Soc. 139*, 1810−1813.

(10) Walton, T., and Szostak, J. W. (2016) A highly reactive imidazolium-bridged dinucleotide intermediate in nonenzymatic RNA primer extension,. *J. Am. Chem. Soc. 138*, 11996−12002.

(11) Wu, T., and Orgel, L. E. (1992) Nonenzymatic template-directed synthesis on hairpin oligonucleotides. 2. Templates containing cytidine and guanosine residues. *J. Am. Chem. Soc. 114*, 5496−5501.

(12) Tam, C. P., Fahrenbach, A. C., Björkbom, A., Prywes, N., Izgu, E. C., and Szostak, J. W. (2017) Downstream oligonucleotides strongly enhance the affinity of GMP to RNA primer-template complexes. *J. Am. Chem. Soc. 139*, 571−574.

(13) Zhang, W., Tam, C. P., Wang, J., and Szostak, J. W. (2016) Unusual base-pairing interactions in monomer-template complexes. *ACS Cent. Sci. 2*, 916−926.

(14) Zhang, W., Tam, C. P., Walton, T., Fahrenbach, A. C., Birrane, G., and Szostak, J. W. (2017) Insight into the mechanism of nonenzymatic RNA primer extension from the structure of an RNA-GpppG complex. *Proc. Natl. Acad. Sci. U. S. A. 114*, 7659−7664.

(15) Kanavarioti, A., Bernasconi, C. F., Doodokyan, D. L., and Alberas, D. J. (1989) Magnesium ion catalyzed P-N bond hydrolysis in imidazolide-activated nucleotides. Relevance to template-directed synthesis of polynucleotides. *J. Am. Chem. Soc. 111*, 7247−7257.

(16) Li, L., Lelyveld, V. S., Prywes, N., and Szostak, J. W. (2016) Experimental and computational evidence for a loose transition state in phosphoroimidazolide hydrolysis. *J. Am. Chem. Soc. 138*, 3986−3989.

(17) Kanavarioti, A., Bernasconi, C. F., Alberas, D. J., and Baird, E. E. (1993) Kinetic dissection of individual steps in the poly(C)-directed oligoguanylate synthesis from guanosine 5′-monophosphate 2-methylimidazolide. *J. Am. Chem. Soc. 115*, 8537−8546.

(18) Kanavarioti, A., Bernasconi, C. F., and Baird, E. E. (1998) Effects of monomer and template concentration on the kinetics of nonenzymatic template-directed oligoguanylate synthesis. *J. Am. Chem. Soc. 120*, 8575−8581.

(19) Kervio, E., Claasen, B., Steiner, U. E., and Richert, C. (2014) The strength of the template effect attracting nucleotides to naked DNA,. *Nucleic Acids Res. 42*, 7409−7420.

(20) Izgu, E. C., Fahrenbach, A. C., Zhang, N., Li, L., Zhang, W., Larsen, A. T., Blain, J. C., and Szostak, J. W. (2015) Uncovering the thermodynamics of monomer binding for RNA replication. *J. Am. Chem. Soc. 137*, 6373−6382.

(21) Kervio, E., Sosson, M., and Richert, C. (2016) The effect of leaving groups on binding and reactivity in enzyme-free copying of DNA and RNA,. *Nucleic Acids Res. 44*, 5504−5514.

(22) Puthenvedu, D., Janas, T., Majerfeld, I., Illangasekare, M., and Yarus, M. (2015) Poly(U) RNA-templated synthesis of AppA. *RNA 21*, 1818−1825.

(23) Majerfeld, I., Puthenvedu, D., and Yarus, M. (2016) Cross-backbone templating; ribodinucleotides made on poly(C). *RNA 22*, 397−407.

(24) Wachowius, F., Attwater, J., and Holliger, P. (2017) Nucleic acids: function and potential for abiogenesis. *Q. Rev. Biophys. 50*, e4.




DOI: 10.1021/acs.biochem.7b00792
*Biochemistry* XXXX, XXX, XXX−XXX